THICK TARGET HYPERVELOCITY IMPACT CRATER MORPHOLOGY: THE INFLUENCE OF IMPACT ANGLE, SPEED AND DENSITY RATIO.

D. J. Gardner and M. J. Burchell

Unit for Space Sciences and Astrophysics, University of Kent at Canterbury,
Canterbury, Kent, CT2 7NR. UK.

ABSTRACT

Thick target impact studies have been performed using the Light Gas Gun facility at the University of Kent at Canterbury to study the effect on the final crater shape of the projectile's density, impact angle and velocity. We compare the preliminary results of these studies with similar results obtained by numerical modelling with the AUTODYN-3D hydrocode. The physical significance of the observed impact features is discussed and implications for spacecraft impact analysis are suggested.

1. NOTATION AND MEASUREMENTS

V	velocity	θ	impact Angle
d_p	particle diameter	T_c	crater depth
D_c	crater diameter	$D_{c_{max}}$	(long axis)
$D_{c_{min}}$	(short axis)	C_c	Circularity

All angles are measured from the normal to the target surface.

All measurements are relative to, or in, the original surface plane. The definitions of these measurements is shown schematically in Fig. 1. The long and short axes of an elongated crater $D_{c_{max}}$ and $D_{c_{min}}$ are the internal bowl diameters measured in the original surface plane. The circularity C_c is defined as $D_{c_{min}}/D_{c_{max}}$. It is 1.0 for a circular crater, tending to 0 with increasing elongation.

2. INTRODUCTION

Any surface exposed to the near-Earth space environment will receive hypervelocity impacts from space-debris and micrometeoroids. The majority of metallic spacecraft surfaces are "semi-infinite", i.e. thick relative to the impacts they receive. Since a surface that covers a larger exposed area *must* receive more impacts (assuming the exposure geometry is unchanged), it follows that the majority of space-debris and micrometeoroid impacts are on thick targets. For spacecraft retrieved from LEO (e.g. LDEF, EuReCa etc.) it is possible to locate and measure the craters resulting from these impacts (Ref. 1, 2). The data then provides information on particle flux in LEO (Ref. 3, 4, for example). Any more detailed analysis (e.g. to obtain impactor velocities, sizes, densities etc.) requires a more sophisticated knowledge of the response of the target (spacecraft)

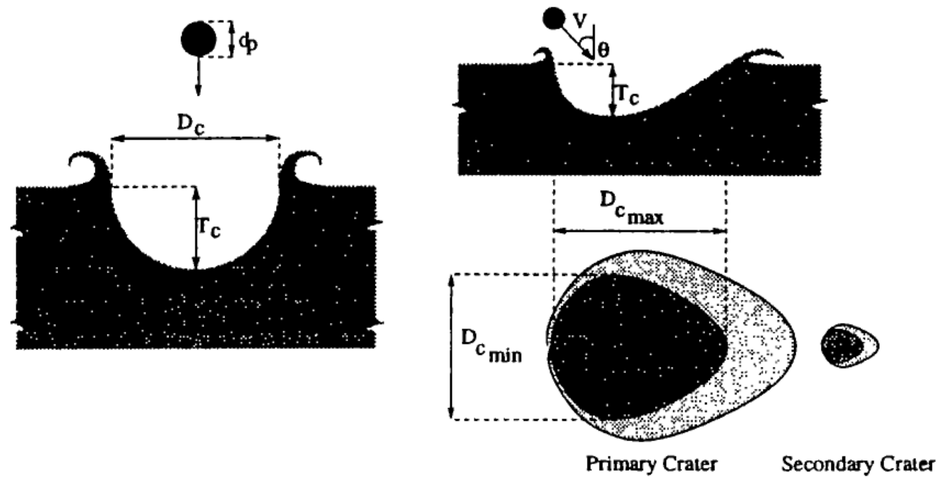

Figure 1: Measurements taken from a hypervelocity impact.

material to hypervelocity impacts. This requires the careful use of calibration data, often from laboratory experiments. Computer-based modelling tools (hydrocodes) may also be used to gain access to parameter ranges and effects (e.g. shock pressures around μm scale events) that would be difficult (or impossible) to achieve in the laboratory. However, the models must first be shown to give good correlation with laboratory impacts.

In this paper we concentrate on the issue of obtaining impact direction from the impact crater. If the obtained direction is combined with a knowledge of the pointing history of the spacecraft, then the possible sources of the flux can be considered.

The analysis of hypervelocity impact craters from retrieved spacecraft surfaces, such as those on NASA's LDEF (Ref. 1, for example) or ESA's EuReCa (Ref. 2) will thus benefit from any addition of fully measured data to the somewhat sparse collection currently published.

3. NUMERICAL MODELLING

Results of numerical modelling by Hayhurst et al. (Ref. 5) and Gardner (Ref. 6) performed using the AUTODYN-3D hydrocode (Ref. 7) are shown in Fig. 2. The calculations were performed for an aluminium 2024 target and 1 μm diameter projectiles of iron, aluminium 2024 and water (where the projectile was a sphere of water with no internal strength). Impact angles were 0°, 50°, 60°, 65°, 75°, 80° and 85°, with velocities of 6.5 km/s (water and aluminium projectiles), 10 km/s (iron and aluminium projec-

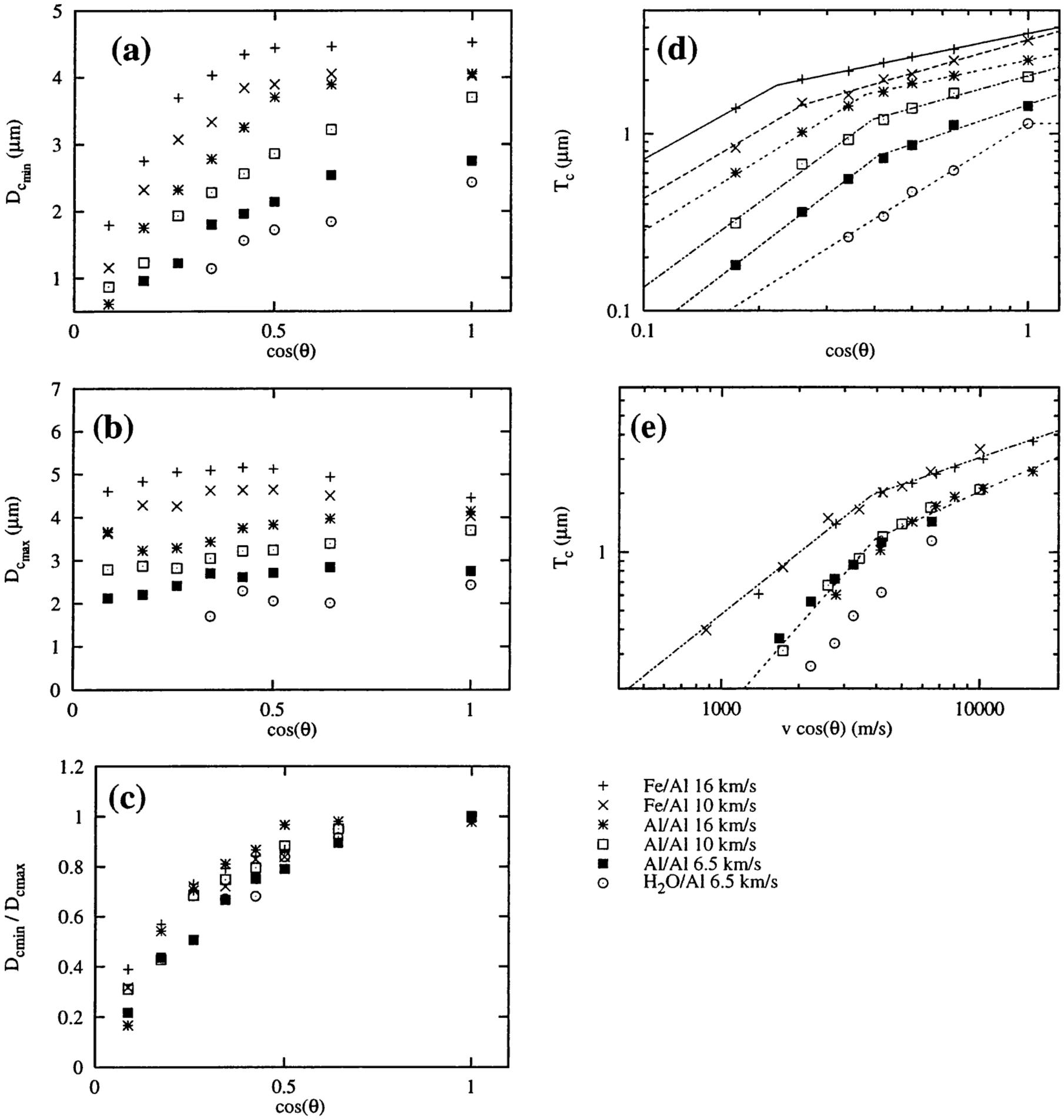

Figure 2: Results of hydrocode modelling of 1μm particle impacting Aluminium.

tiles) and 16 km/s (iron and aluminium projectiles).

The following features are noted:

- The short crater diameter $D_{c_{min}}$, demonstrates a fairly constant behaviour in all cases until almost 60° (Fig. 2a). After this there is then a rapid reduction with increasing impact angle.
- The long crater diameter $D_{c_{max}}$, is largely unaffected by impact angle (Fig. 2b). For the iron particles there is an initial slight increase with angle, peaking at 65° and then falling. For the other projectiles $D_{c_{max}}$ remains approximately constant for $\theta < \theta_{crit}(60°)$ and thereafter a gradual reduction is seen.
- The circularity is shown in Fig. 2c. In all cases it falls only slightly as impact angle increases from 0° to 60°. From the results for Al/Al at various velocities, this fall off is less severe the greater the velocity. Above 60° there is a rapid decrease in circularity in all cases. In this high angle region no trend is seen favouring any projectile/target combination or impact velocity.
- Crater depth T_c is shown in Fig. 2d. The data is fitted by a power law, with separate powers below and above a critical angle θ_{crit}. At this

Projectile	Velocity km/s	θ_{crit}	Power law	
			$\theta < \theta_{crit}$	$\theta > \theta_{crit}$
Aluminium	16	68	0.46	1.33
Aluminium	10	67	0.61	1.59
Aluminium	6.5	66	0.74	1.66
Aluminium	*all*	-	0.60	1.51
Iron	16	77	0.45	1.2
Iron	10	75	0.63	1.27
Iron	*all*	-	0.48	1.2
Water	6.5	-	-	1.36

Table 1: Critical angles and power law dependencies for crater depths obtained from the modelling. Also shown are the power laws from the combined ($V \cos\theta$) plots.

point there is a "knee" in the data after which the depth reduces at a more rapid rate (see Table 1 for values found by the fit). This critical angle has also been observed by several authors and by investigation with hydrocode modelling (Ref. 5) has been found to correspond to material from the projectile leaving the impact area as a result of particle shear or skipping. θ_{crit} appears to be dependent on the impactor material, indeed for the zero-strength case of water this regime is found to apply at all impact angles.

- There is no single fit for the various projectile/target and impact velocity combinations. To investigate further we show T_c vs. $V \cos\theta$ (V is impact velocity) in Fig. 2e. We find that for all Al/Al data a single fit is now possible, as is one for Fe/Al. The slopes of the fits are given in Table 1. For Al/Al we find the "knee" at $V \cos\theta \simeq 3500$ m/s, whereas it is ~3800 m/s. for Fe/Al.

4. EXPERIMENTAL RESULTS

The Light Gas Gun (LGG) facility at the University of Kent (Ref. 8) has been used to perform a number of impact programmes on inclined metallic targets. Projectile and target combinations are given in Table 2 (where Cell. Ace. refers to cellulose acetate, density 1360 kg/m^3, and St.St is stainless steel). Impact angles were 0°, 10°, 20°, 30°, 40°, 50°, 55°, 60°, 65°, 70°, 75° and 80°. The impact speed was 5.13 ± 0.12 km/s.

Experimental measurements were performed using an optical microscope with all three axes equipped with displacement gauges (± 3 μm accuracy). Errors on the measurements are dependent on judgement, and are estimated at 20 μm in $D_{c_{max}}$ and $D_{c_{min}}$ and 50 μm in T_c. When presenting the data we have normalized all results to projectile diameter d_p.

Projectile	Diameter mm	Target
Cell. Ace.	1.5	Al
St. St	1.0	Al
St. St	1.0	St. St.
St. St	1.0	Lead

Table 2: Projectile and target combinations of the experimental programme.

While at different velocities and scales, the results, shown in Fig. 3, show the same general trends as were identified in the modelling programme. Fig. 4 shows the crater shapes from impacts of stainless steel on stainless steel.

- The crater minor axis $D_{c_{min}}$ (Fig. 3a) shows a critical angle at around 60°, after which there is a rapid reduction. This is not true for the major axis $D_{c_{max}}$ (Fig. 3b), where only St.St./Al shows a critical angle (again around 60°). In the other projectile/target combinations $D_{c_{max}}$ varies uniformly with $\cos\theta$.

- Circularity (Fig. 3c) shows critical angles for all the data except St.St./Al. The results of fits to the data are given in Table 3. It can be seen that θ_c depends on the projectile/target combination, and can vary by 18°.

- Crater depth T_c (Fig. 3d) also shows a critical angle effect, except for Cell.Ace/Al (results of fits to the data are given in Table 3). Once more we find that θ_c depends on the projectile/target combination, with a range of 16° in the values found. Further, we note that the values are not the same as those for the critical angles affecting the circularity. The depths for St.St/Al and St.St/Pb are very similar. Standard parameterizations (Ref. 9, for example) show that depth depends on both target density and strength (or hardness), for aluminium and lead these compensate for one another giving near equal depths. In Fig. 3e we show T_c as a function of $V \cos\theta$, where we have also added data from Christiansen et al. (Ref. 10) for Al/Al at 6.5 to 7 km/s. There is no data at two velocities for the same projectile/target combination, although we note that for the two cases of projectile and target being the same (Al/Al and St.St./St.St.) the data are almost indistinguishable.

- At angles above about 60° a secondary crater begins to form, initially merged with the main crater, but a higher angles becoming clearly sep-

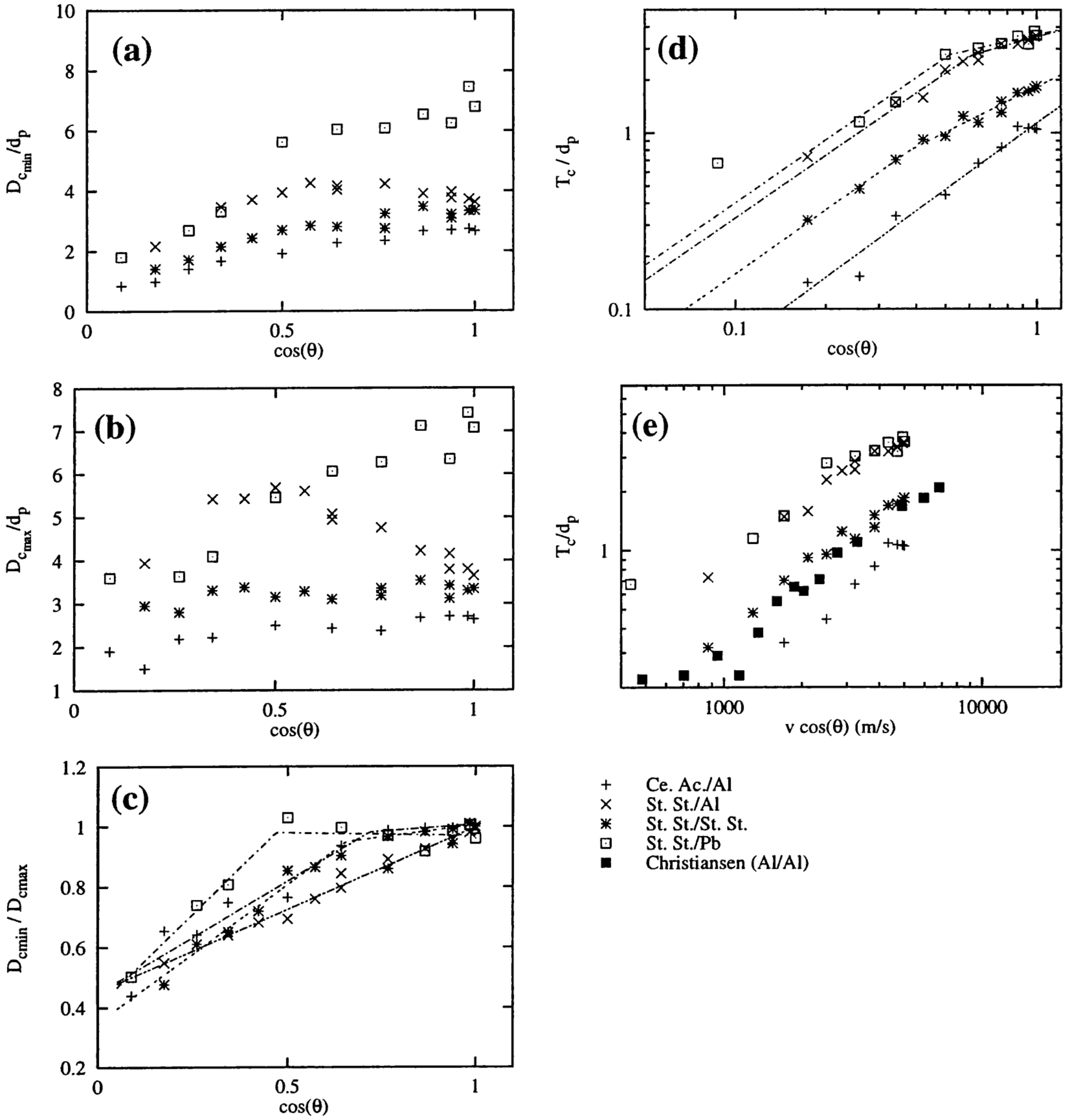

Figure 3: Results of experimental programme.

arated. As seen in Table 3, the precise angle at which this phenomena is observed is dependent on the projectile and target combination. A similar effect for highly oblique impacts on thin foils was found by Schonberg et al. (Ref. 11). Christiansen et al. (Ref. 10) attributed it to the spallation of the particle, leading to the top part of the particle impacting at a different angle. Hayhurst et al. (Ref. 5), however, found that spallation was not necessary and a particle could break up and cause secondary cratering simply due to the shear forces on the different parts of the projectile.

- We note that a "spray" of down-stream damage is observed (~10°) before the formation of a secondary crater is observed.

5. CONCLUSIONS

At least 2 critical angles have been found in both sources of data describing the onset of rapid changes in crater circularity and depth. These angles vary significantly for various projectile/target combinations, and, for any given combination, the critical angle for circularity is not the same as that for depth. Further, not all projectile/target combinations dis-

Projectile	Target	T_c Power law			C_c Fit			Secondary craters	
		θ_{crit}	α_1	α_2	θ_{crit}	a_1	a_2	First observed	Separated
Cell. Acetate	Al	0°	-	1.25	44°	0.091	0.742	75°	80°
Stain. steel	Al	52°	0.48	1.17	0°	0	0.545	75°	85°
Stain. steel	Lead	59°	0.43	1.18	62°	-.021	1.225	75°	85°
Stain. steel	St. st	68°	0.86	1.2	49°	0.163	0.912	65°	75°

Where: $T_c \propto \begin{cases} \theta < \theta_{crit} : (\cos\theta)^{\alpha_1} \\ \theta > \theta_{crit} : (\cos\theta)^{\alpha_2} \end{cases}$ and $C_c = \begin{cases} \theta < \theta_{crit} : a_1 \cos\theta + constant \\ \theta > \theta_{crit} : a_2 \cos\theta + constant \end{cases}$

Table 3: Critical angles and $\cos\theta$ dependancies for crater depths and circularities obtained from the experimental programme.

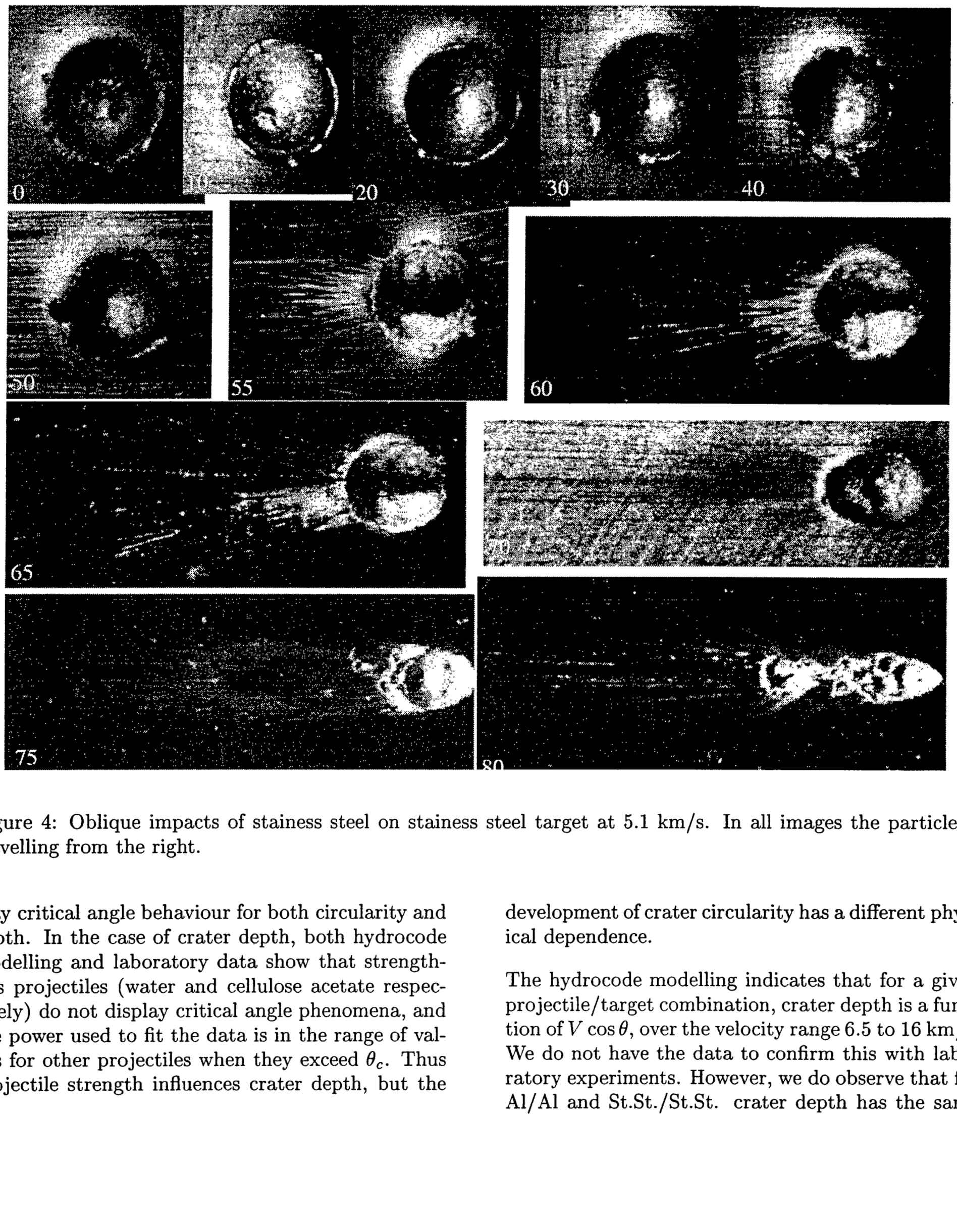

Figure 4: Oblique impacts of stainess steel on stainess steel target at 5.1 km/s. In all images the particle is travelling from the right.

play critical angle behaviour for both circularity and depth. In the case of crater depth, both hydrocode modelling and laboratory data show that strengthless projectiles (water and cellulose acetate respectively) do not display critical angle phenomena, and the power used to fit the data is in the range of values for other projectiles when they exceed θ_c. Thus projectile strength influences crater depth, but the development of crater circularity has a different physical dependence.

The hydrocode modelling indicates that for a given projectile/target combination, crater depth is a function of $V\cos\theta$, over the velocity range 6.5 to 16 km/s. We do not have the data to confirm this with laboratory experiments. However, we do observe that for Al/Al and St.St./St.St. crater depth has the same

dependence on $V \cos\theta$.

We now consider the implications of these results as regards impacts on spacecraft. These impacts will be by projectiles of unknown size, density, velocity and inclination. If we wish to extract impact angle from measured craters we clearly cannot use a single parameter, such as length, depth, etc. but must use a more general characteristic such as circularity.

The hydrocode modelling of μm sized aluminium particles shows that as velocity varies from 6.5 to 16 km/s the circularity can vary by ± 0.1 at a given angle. The resultant uncertainty in the reconstructed impact angle ($\theta_{\text{reconstructed}}$) is dependant on θ, but if θ were 60° the resultant spread of circularities would lead to the range $0° < \theta_{\text{reconstructed}} < 70°$. The sensitivity improved dramatically for larger θ, where if θ were really 78° the observed range in circularity would be decoded to the range $72° < \theta_{\text{reconstructed}} < 84°$.

Thus even without a knowledge of impact velocity circularity is a fairly accurate indicator of impact angle for large angle impacts. If the projectile type is allowed to be unknown this worsens slightly, but no enough to invalidate this result. This is confirmed by the light gas gun data at 5.3 km/s.

The appearance of secondary craters at large impact angles is also of significance. If one simply counts craters in order to obtain a flux, the total crater count effectively counts large angle craters more than once. In the laboratory we observed multiple secondary craters associated with large angle impacts, some of which were clearly separated from the mail crater. These secondary craters can be at a distance from the main impact of several times the major axis of the main crater. Separation occurs for $\theta > 75°$ (Table 3) corresponding to circularities of < 0.7. The presence in a data-set of craters with $C_c < 0.7$ should thus indicate probable overcounting and a correction will have to be applied. A test if this is necessary would be to measure the crater population density in areas adjacent to craters with $C_c \simeq 1.0$ and $C_c < 0.7$. The magnitude of such a difference will indicate the degree of correction necessary.

It is to be noted that non-spherical particles can also be a cause of low circularity and other measurements, such as crater depth and lip profile, should also be considered to avoid mistaken classification.

REFERENCES

1. Love, S. G. et al., Morphology of meteoroid and debris impact craters formed in soft metal targets on the LDEF satellite, *Int. J. Impact Engng.*, Vol. 16, No. 3, 405–418, 1995.

2. Gardner, D. J. et al., Micro-particle impact flux on the Timeband Capture Cell Experiment of the Eureca Spacecraft, *Adv. Space Res.*, Vol. 17, No. 12, 193–199, 1996.

3. McDonnell, J. A. M. and Gardner, D. J., Meteoroid morphology and densities: decoding satellite impact data, *Icarus*, In submission, 1997.

4. McDonnell, J. A. M. et al., Microparticle populations at LEO altitudes: recent spacecraft measurements, *Icarus*, Accepted for publication 1997.

5. Hayhurst, C. J. et al., Modelling of microparticle hypervelocity oblique impacts on thick targets, *Int. J. Impact Engng.*, Vol. 17, 375–386, 1995.

6. Gardner, D. J., *Hypervelocity Impact Morphology*, Ph.D. thesis, University of Kent at Canterbury, 1995.

7. Birnbaum, N. K. et al., AUTODYN - an interactive non-linear dynamic analysis program for microcomputers through supercomputers, *Proc. 9th International Conference on Structural Mechanics in Reactor Technology*, Lausanne, 1987.

8. Burchell, M. et al., The hypervelocity impact facilities at the university of Kent at Canterbury. UK, *Workshop on particle capture, recovery and velocity trajectory measurement technologies, LPI Tech. Rpt. 94-05*, editor M. E. Zolensky, Lunar and Planetary Insitute, Houston, 1993.

9. Shanbing, Y. et al., Experimental laws of cratering for hypervelocity impacts of spherical projectiles into thick targets., *Int. J. Impact Engng.*, Vol. 15, No. 1, 67–77, 1994.

10. Christiansen, E. L. et al., Highly oblique impacts into thick and thin targets, *Int. J. Impact Engng.*, Vol. 14, 157–168, 1993.

11. Schonberg, W. P. et al., Hypervelocity impact physics, NASA contractor report 4343, 1991.